Comprehensive Eliashberg analysis of microwave conductivity and penetration depth of K-, Co-, and P-substituted

High Dynamic Performance Power Quality Conditioner for AC Microgrids

Asif Raza Jarwar[1], Amir Mahmood Soomro[1], Zubair Ahmed Memon[1], Shafiq Ahmed Odhano[2*], Muhammad Aslam Uqaili[1], Abdul Sattar Larik[1]

[1] Department of Electrical Engineering, Mehran University of Engineering and Technology, Jamshoro 76062, Pakistan
[2] Department of Electrical and Electronic Engineering, University of Nottingham, University Park, Nottingham NG7 2RD, United Kingdom
[*] shafiq.odhano@nottingham.ac.uk

Abstract: This paper deals with power quality problems encountered in weak ac microgrids and solutions for mitigation. A power electronic converter can be used as an effective power quality conditioner to compensate non-idealities in currents drawn from the grid. A power quality conditioner consisting of three power converters connected to a common dc link is analysed. One of these converters acts as an active power filter for removing unwanted harmonics in grid currents feeding a non-linear load. The other two converters instead remove the harmonics from the voltage at the terminals of a sensitive load. The control of the shunt converter is designed to be fast enough for power quality servicing but also has a fast disturbance rejection capability. Simulation and experimental results validating the concept are provided along with obtained total harmonic distortion improvements.

1. Introduction

A microgrid, whether ac or dc, is a local electricity distribution system that is operated in a controlled way and includes both electricity users and electricity generation. Usually, the generation is through renewable energy resources consisting of small scale distributed generation (DG) sources [1]. While a dc microgrid hosts energy resources, such as photovoltaics and batteries as direct coupling and wind farms through power electronic interface, and supplies loads in dc [2], [3], an ac microgrid can have a direct coupling with the main utility grid [4], [5] when supplying loads in conjunction with the distribution grid or it can be on its own e.g. in islanding mode. With greater penetration of DG, microgrids emerge as a viable alternative to conventional utility grids in providing reliable and secure power supply. However, increasing penetration of small DG sources does bring some technical challenges with regards to protection, control and power quality of microgrids. The power quality issues encountered in these microgrids are mainly due to the reduced power capacity of the generation resources powering them which cannot constitute a robust system. A grid simulator for assessing such power quality issues in ac microgrids is presented in [6] that replicates the conditions occurring in practical networks. International standards such as IEEE-1159-1995, IEC-61000 part 2 and 3, EN 50160 define acceptable limits on harmonic distortion and voltage variations that must be respected in all public utility networks. A micro-grid supplying a group of consumers constitutes a public utility network that must obey these normative limits.

The power quality issues in microgrids can be handled by installing harmonic filters. These filters can either be composed of passive components, e.g. capacitors and inductors, or they can be active power filters making use of the state-of-the-art power electronics. Passive filters are bulky and introduce power losses that can have grave consequences on the efficiency of small scale systems such as a microgrid. The use of active power filters is privileged due to their capability of correcting various disturbances and that too with high dynamics and maintaining higher overall efficiency.

The literature reports a number of works for the control of power electronic converter for power quality servicing. The work presented in [7] studies the dc-link voltage control of a back-to-back active power conditioner that interfaces two microgrids. Two control strategies namely the optimal ac-line current regulation and dynamic dc-link voltage regulation are analysed. The authors have shown that a bidirectional power transfer can be obtained by controlling the dc-link voltage with both these strategies while maintaining sufficiently clean ac side currents on both sides of the power conditioner. It has been shown that without

dynamic dc-link voltage control it is not possible to handle large power increases or decreases at any one port. A micro-grid power quality enhancement through three-phase four-wire power converters is proposed in [8]. A pair of converters is used at each node connecting a DG source with a utility grid. One of the converters is connected in shunt to ensure balanced voltages in the microgrid while the other, in series, eliminates disturbances in voltage by injecting negative- and zero-sequence voltages. The control of shunt converter is achieved through a proportional-resonant controller as outer voltage control loop with inner current control loop for the filter inductor. For the series converter, the control consists of a proportional-resonant controller each for negative and zero-sequence and a flux-charge model control is proposed for limiting the currents during utility voltage sags.

A multi-objective control strategy for multi-functional grid-connected inverters is presented in [9]. The multi-functional converter serves as a renewable energy integration interface as well as for power quality enhancement. The inner control loop of this converter consists of a proportional-resonant controller similar to [8]. The reference values for this inner loop are generated through a multi-objective function which is based on comprehensive power quality evaluation index. This index is based on catastrophe decision theory and takes into account the total harmonic distortion and the true power factor. The authors have demonstrated control performance for non-linear load current compensation as well as under active and reactive power variations.

An active power filter consisting of four-leg voltage source inverter (VSI) for power quality improvement in renewable power generation setting was used in [10]. The control was implemented through predictive current control of each of the three phase currents and that of the neutral leg through minimization of a cost function. The switching state that minimized the cost function was applied directly through the inverter switches. Since there was no modulator, the switching frequency was variable that could be a problem for the design of filters for electromagnetic interference.

In [11], an ac microgrid is constructed of two VSIs coupled through inductive-capacitive (LC) output filters. As in [10], the control is implemented through finite control set model predictive control with the addition of derivative of filter capacitor voltage to improve tracking dynamics of output voltage control. Again, as the modulator is not used so the switching frequency is not constant even through the authors added a term for minimizing the switching frequency. However, a low switching frequency compromises the quality of output voltage waveforms.

In this paper, we study the control of a power quality conditioner (PQC) for an ac microgrid through a different control strategy than [10], [11]. The system under consideration consists of three power electronic converters connected to a common dc-link. Each converter is interfaced with the ac microgrid through an inductive-capacitive (LCL) filter. This filter prevents the commutation frequency harmonics from making their way into the ac network. A deadbeat current control strategy is preferred over traditional proportional-integral controllers for its high dynamic response and over model predictive control for its constant switching frequency operation. The paper presents results for power quality conditioning of different loads with various power quality issues.

2. System Description

Fig. 1 shows the system under study where F1, F2 and F3 denote the three incoming feeders from the grid and Load1, Load2 and Load3 are cumulative loads on the feeders seen at the point of common coupling. In this particular configuration, the converters numbered 1 and 2 compensate the voltage harmonics at the terminals of loads 1 and 2, respectively, while the converter 3 compensates the distortions in grid currents caused by load 3. Thus converters 1 and 2 are series compensators while converter 3 is a shunt compensator. The system of Fig. 1 can be reconfigured in a number of other ways for achieving current and voltage harmonics compensation of the three loads. The LC filter ($L_f C_f$) for converters 1 and 2 is necessary for compatibility reasons as they will be controlled in voltage. However, the filter arm ($C_f L_2$) for converter 3 can be omitted leaving behind only L_f, which is sufficient for interfacing the converter with the ac network.

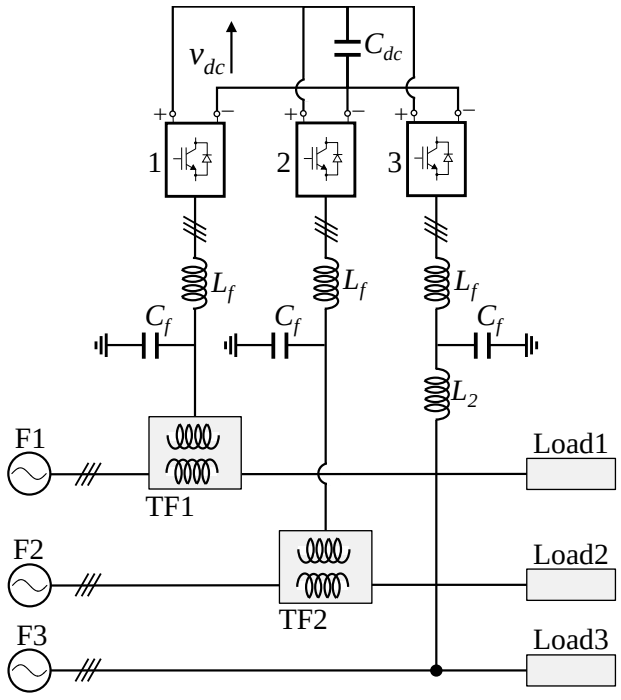

Figure 1. Single-line diagram of the system under study.

As can be observed from Fig. 1, there is no external source that maintains the dc-link voltage. Therefore, it becomes necessary to sustain the dc-link through one of the converters. Since converters 1 and 2 are controlled in voltage, only converter 3, which must be controlled in current to compensate current harmonics, can provide power

for maintaining the dc-link voltage to a suitable level. Converter 3 thus works as an active rectifier for keeping the dc-link voltage constant while, at the same time, injecting current that compensates distortion caused by the load. This makes it imperative that the control of converter 3 has a sufficiently high bandwidth. Additionally, as the current compensation for non-linear loads may also require the injection of high frequency current components, the bandwidth of the controller plays a vital role in deciding the quality of compensation.

3. Control Strategy

3.1. *Converter 1 and 2 Voltage Control*

The series converters 1 and 2 are voltage controlled. The reference voltage is generated based on the measured voltage at F1 and F2. Let the amplitude of the required sinusoidal phase voltage at the terminals of loads 1 and 2 be V_R. If it is assumed that the *d*-axis of an arbitrary rotating reference frame coincides with phase U of the load voltage, then the required voltage vector in the *dq* frame can be written as:

$$v_d + jv_q = V_R + j0 \tag{1}$$

And in the stationary αβ frame, the required voltage will be given by:

$$\begin{bmatrix} v_\alpha \\ v_\beta \end{bmatrix} = \begin{bmatrix} \cos\vartheta & -\sin\vartheta \\ \sin\vartheta & \cos\vartheta \end{bmatrix} \begin{bmatrix} v_d \\ v_q \end{bmatrix} \tag{2}$$

where ϑ is the angle of rotation of the arbitrary reference frame. Eq. (2) when transformed into phase quantities will give:

$$\begin{bmatrix} v_U \\ v_V \\ v_W \end{bmatrix} = \begin{bmatrix} 1 & 0 \\ -\frac{1}{2} & \frac{\sqrt{3}}{2} \\ -\frac{1}{2} & -\frac{\sqrt{3}}{2} \end{bmatrix} \begin{bmatrix} v_\alpha \\ v_\beta \end{bmatrix} \tag{3}$$

Now, if the measured phase voltages contain any harmonics, the compensation required of converter 1 or 2, in terms of phase quantities, is:

$$v_U^* = v_U^m - v_U \tag{4}$$

where the superscript '*m*' stands for measured and * represents the reference voltage for converter 1 or 2. Eq. (4) gives only phase U voltage, the remaining two phases will have similar expressions.

3.2. *Current Control of Converter 3*

The control of the shunt converter 3 needs careful attention as it is responsible for maintaining the dc-link voltage as well as for current distortion compensation. In fact, the sub-system constituted by the interface of converter 3 with the grid is a typical topology of voltage source inverter with LCL filter. The control of this topology has been studied in depth in the literature [12]–[17]. In this paper, the interface of converter 3 with the grid is simplified by removing the additional branch ($C_f L_2$), although that does deteriorate the power quality conditioning performance. The exclusion of this branch brings two advantages: (i) there will be no current and voltage sensors required for L_2 and C_f state variables' measurement and (ii) the control design problem will become extremely simple.

Before writing equations for current control, it is necessary to define the convention used for the direction of current (and hence power). Let the converter 3 be a consumer such that the direction of current is towards dc-link from the grid feeder 3. Fig. 2 defines this convention. In Fig. 2, R_f is the series resistance of the filter inductance L_f.

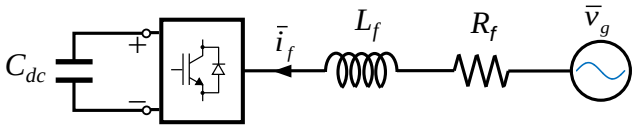

Figure 2. Convention used for converter 3.

First, the controller for dc-link voltage is described. It must be noted that an active rectifier needs to maintain dc-link voltage only by drawing active power from the grid keeping reactive power close to null. So, if the grid voltage $\bar{v}_g$ is chosen as reference vector whose angle ϑ is used as the angle of the *dq* rotating reference frame, then the active power, in terms of *dq* quantities, will be given by:

$$P = \frac{3}{2}\left(v_{gd} i_d + v_{gq} i_q\right) \tag{5}$$

where the peak value invariant transformation of (3) is used. It can immediately be observed that if ϑ is aligned with the grid voltage vector then, by definition, $v_{gq} = 0$. Thus the active power can only be controlled by controlling i_d. Furthermore, keeping $i_q = 0$ will ensure no reactive power is drawn from the grid. So, i_d must be used to control dc-link voltage. The transfer function for dc-link voltage control can be written as:

$$\frac{V_{dc}}{i_d} = \frac{1}{C_{dc} s + 1/R_{dc}} \tag{6}$$

here R_{dc} is equivalent parallel resistance across dc-link capacitance that signifies dc load, such as current drawn by converters 2 and 3. As its value is not precisely known, for control design it can also be neglected i.e. $R_{dc} = \infty$ and any current drawn from dc-link acts as a disturbance.

A proportional-integral controller is used for controlling the dc-link voltage here whose bandwidth decides the controller dynamics. For the internal current control loop, a fast controller is needed for two reasons: (i) the dc-link controller assumes an ideal internal loop so the bandwidth of current control must be at least an order of magnitude higher than outer voltage control loop; (ii) the load current harmonics usually occur at higher frequency that must be

compensated by the controller. For these reasons a deadbeat control loop is used in this paper for its fast dynamics.

Referring to Fig. 2, the voltage equation of the system can be written as:

$$\bar{v}_g = R_f \bar{i}_f + L_f \frac{d\bar{i}_f}{dt} + j\omega L_f \bar{i}_f + \bar{v}_{conv} \tag{7}$$

here ω is the angular frequency of the rotating reference frame and the vector $\bar{v}_{conv}$ denotes the voltage applied by the converter. For applying a deadbeat control, (7) is discretized using Euler's approximation for the current derivative terms as:

$$\bar{i}_f(k+1) = \left(1 - \frac{R_f T_s}{L_f}\right)\bar{i}_f(k) - j\omega T_s \bar{i}_f(k) + \frac{T_s}{L_f}\left(\bar{v}_g(k) - \bar{v}_{conv}(k)\right) \tag{8}$$

where T_s is the sample time and k denotes the discrete sampling instants. Eq. (8) is used for current prediction at the next sampling instant ($k + 1$). The control action applied at the next switching instant is computed by rearranging (8) as:

$$\bar{v}_{conv}(k+1) = -R_f \bar{i}_f(k+1) - \frac{L_f}{T_s}\left(\bar{i}_f^{*} - \bar{i}_f(k+1)\right) - j\omega L_f \bar{i}_f(k+1) + \bar{v}_g(k+1) \tag{9}$$

In (9) the superscript * represents the reference current vector obtained as a combined action of dc-link voltage regulator as well as the components of current to be compensated for load. Eq. (9) ensures that the current reference is reached in one sampling time (ideally) if it is within the dc-link voltage limits. However, in digital implementation, the digital delay causes an additional T_s delay. This delay must be appropriately compensated for correct prediction of currents at the next sampling instant through (8) [18]. It must be noted that as the deadbeat control action computed from (9) does not contain any integrative term as in a PI regulator, the control performance depends heavily on parameters such as L_f, R_f and also the error caused by inverter dead-time effects. A small integrative term can be added for disturbance rejection to remove any steady state error through adaptive load model as done in [19].

Let us see the reference current generation for (9). As mentioned above the reference current consists of two parts, the first is provided by the dc-link PI controller based on the plant of (6) and the second comes from the load current harmonics to be eliminated. As the purpose of shunt converter is to supply only the harmonics of load current while the fundamental component is drawn from the grid, it is necessary to identify these harmonics. A simple way is to measure the load current for load 3 in Fig. 1 and then identify its fundamental component and harmonics. If the transformation of (2) is applied on the measured load currents to get their *dq* components as:

$$\begin{bmatrix} i_{Ld} \\ i_{Lq} \end{bmatrix} = \begin{bmatrix} \cos\vartheta & \sin\vartheta \\ -\sin\vartheta & \cos\vartheta \end{bmatrix} \begin{bmatrix} i_{L\alpha} \\ i_{L\beta} \end{bmatrix} \tag{10}$$

The fundamental component of load current appears as a constant in the *d*-axis while all the harmonics are superimposed on both *d*- and *q*-axis components. To separate the fundamental frequency component a low-pass filter can be used and the current required of the shunt converter can be written as:

$$\begin{aligned} i_d^{*} &= i_{dc}^{*} + i_{Ld} - LPF\left(i_{Ld}\right) \\ i_q^{*} &= i_{Lq} \end{aligned} \tag{11}$$

here i_{dc}^{*} is the current reference generated by the dc-link voltage controller.

It can be observed from (2), (5), (9) and (10) that the identification of angle ϑ plays a significant part in the overall performance of the control. A phase locked loop (PLL) can be used for getting the grid voltage angle very accurately. However, a PLL works well only when there is no disturbance in the grid voltage. An ac microgrid by definition is weak which means its voltage may contain harmonics and the PLL will not be able to filter them out. A resonant filter tuned at the grid frequency can be used to avoid any grid voltage harmonics from polluting the angle ϑ and, thus, the *dq* currents obtained from (10). The following resonant filter is used in this paper:

$$G_{res} = \frac{k_{res} s}{s^2 + k_{res} s + \omega^2} \tag{12}$$

where the resonance frequency ω is set equal to the grid fundamental frequency and k_{res} is the filter gain.

4. Performance Evaluation

The performance of the above controller is verified for power quality conditioning in a microgrid that supplies loads causing harmonic distortion in currents and voltages. The system of Fig. 1 is constructed in Matlab Simulink through basic blocks. Table-I summarizes simulation parameters used. Furthermore, the performance of shunt power quality conditioner is also evaluated experimentally on the configuration of Fig. 2 with system parameters given in Table-II. It should be noted that the grid voltage is not a standard value in Table-II as it is supplied through an autotransformer. Besides, the input inductance of the grid is decided by the voltage ratio of the autotransformer and feeding grid, therefore the grid inductance and resistance values are given as estimates. For simplicity, a resistive load on the dc-side in Fig. 2 is added to emulate currents drawn by converters 1 and 2 of Fig. 1.

4.1. Simulation Analysis

In simulations, for loads 1 and 2, the harmonic distortion in voltage is compensated for through converters 1 and 2. The disturbance compensation capability is also analysed for voltage sags and swells. For the shunt converter 3 the performance of deadbeat current controller is decisive in the

current compensation capability of the converter. It is analysed in detail in the following.

Harmonic content in the currents drawn from the grid is caused by non-linear loads such as a transformer in no-load condition that introduces third and fifth harmonics in current or a diode rectifier circuit that introduces odd harmonics (except the multiples of third). For emulating a non-linear load, the diode rectifier supplying an inductive load of Fig. 3 is connected in parallel with load 3 of Fig. 1. An input inductance is connected at the input of the rectifier for ripple reduction.

Table I: SIMULATION DATA

Grid parameters	
Voltage	380 Vrms (L–L)
Frequency	50 Hz
Inductance	0.45 mH
Resistance	0.2 Ω
Load 1 and 2 parameters	
Inductance	100 mH
Resistance	25 Ω
Load 3 parameters	
Inductance	19.7 mH
Resistance	32 Ω
Rectifier input inductance	0.3 mH
Rectifier dc-side inductance	21 mH
Rectifier dc-side resistance	37 Ω
Power quality conditioner parameters	
Switching/sampling frequency	20 kHz
Filter capacitance	470 μF
Filter inductance Conv 1, 2	0.45 mH
Filter inductance Conv 3	4.5 mH

Table II: EXPERIMENTAL SETUP DATA

Grid parameters	
Voltage	106 Vrms (L–L)
Frequency	50 Hz
Inductance (estimated)	45 μH
Resistance (estimated)	0.04 Ω
DC-side parameters	
Capacitance (C_{dc})	1.88 mF
Resistance	56.7 Ω
Power quality conditioner parameters	
Sampling frequency	20 kHz
Switching frequency	10 kHz
Filter inductance (L_f)	3.0 mH
Series resistance of L_f	0.2 Ω

Fig. 4 shows voltage distortion compensation of converter 1. The compensation is enabled at $t = 0.04$s and a voltage swell of 20% is introduced between $t = 0.06$s and $t = 0.1$s. Fig. 5 shows the Fast Fourier Transform (FFT) plot of voltage harmonics before and after compensation. Before compensation is enabled, the load voltage contains 8th, 10th and 11th harmonics that cause the THD before compensation to be about 16% which after compensation is 4.25%. Also, the voltage amplitude correction is evident during grid voltage swell. Similarly, Fig. 6 and 7 give the voltage compensation performance of converter 2. The load voltage contains 8th, 11th and 13th harmonics with a THD of 17% while after compensation the THD is under 5%. Unlike load 1 where a voltage swell is applied, here a voltage sag of 20% is introduced between $t = 0.06$s and $t = 0.1$s which is effectively mitigated in load voltage.

Generally, only odd harmonics are present in power systems, however, the analysis here is presented also for even harmonics. Asymmetric loads, such as half-wave rectifiers, half-controlled converters, arc furnaces or electrical discharge devices, inject currents with even harmonics in the grid and the voltage drops caused by these currents pollute the grid voltage with even harmonics [20], [21]. The even harmonic components are included in this paper to render the solution more generic and applicable in case of high concentration of asymmetric loads on a given microgrid.

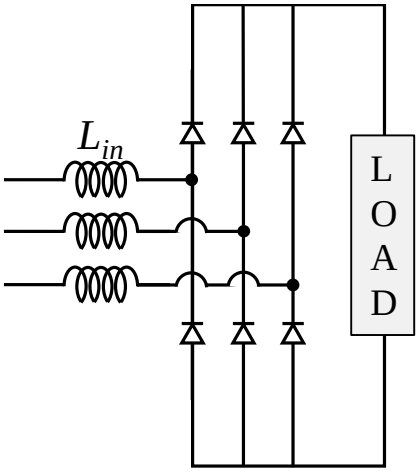

Figure 3. Non-linear load for feeder 3.

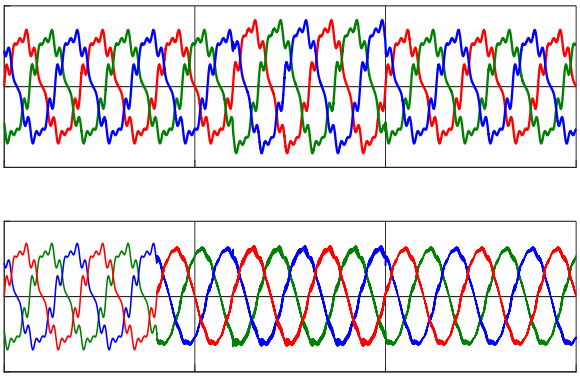

Figure 4. Load 1 voltage compensation – top: distorted grid voltage, bottom: load voltage before and after compensation.

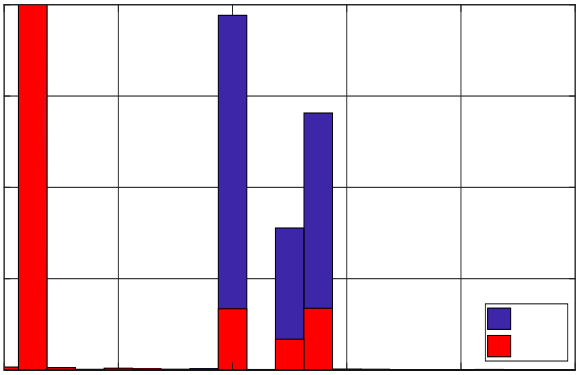

Figure 5. Frequency spectrum of voltage at load 1 before and after compensation – THD before compensation: 16.25%, after: 4.25%.

The performance of converter 3 is analysed in greater detail due to its important role in the overall system. Fig. 8 top plot shows the dc-link voltage control that is controlled from an initial value of 600 V to 650 V. In the bottom plot, the *d*-axis current control is given. It should be noted that the reference *d*-axis current is given by (11) where the fluctuations at six times the fundamental frequency are due to current drawn by diode rectifier (shown later in Fig. 10). Fig. 9 shows current control performance along *q*-axis. It can be observed that the *q*-axis current as given by (11) has a typical diode rectifier trend. The variation is at six times the grid frequency that makes it challenging to follow such a highly distorted waveform. However, the deadbeat controller action of (9) ensures a very good current following.

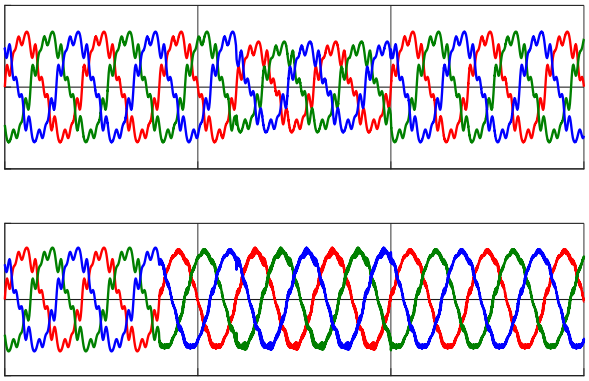

Figure 6. Feeder 2 voltage compensation – top: grid voltage, bottom: load voltage before and after compensation.

Fig. 10 presents the grid currents drawn by the loads of feeder 3 before and after compensation. It can be seen that due to the presence of diode rectifier of Fig. 3, the currents are highly distorted. The effectiveness of compensation is seen after $t = 0.2$s. It must be noted that both the dc-link voltage control and load current compensation are enable simultaneously. The initial dip in grid currents is due to the *d*-axis current of Fig. 8 (refer to the convention defined in Fig. 2). The spikes visible at rectifier commutation points are due to the reversal in *q*-axis current of Fig. 9 which is impossible to follow with limited dc-link voltage. Fig. 11 gives the frequency spectrum of grid currents before and after compensation. It can be seen that the diode rectifier causes all the odd harmonics (except multiples of three) in the grid current. The lower order harmonics are effectively reduced thanks to the high bandwidth of the deadbeat current controller, however, the higher order harmonics 29th onwards are not suppressed much which is understandable with a limited dc-link voltage. Finally, Fig. 12 shows the phase currents injected by the converter 3 to compensate current distortions caused by non-linear load on feeder 3.

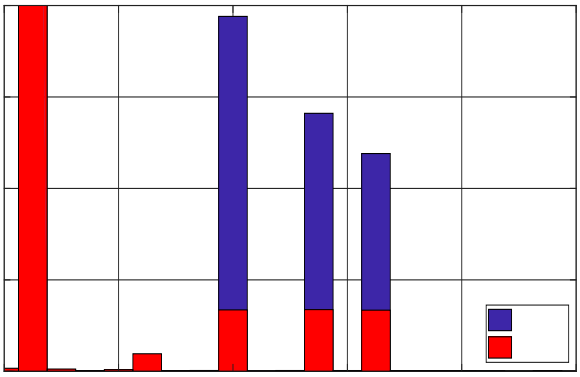

Figure 7. FFT of load 2 voltage before and after compensation – THD before compensation: 17.26%, after: 4.73%.

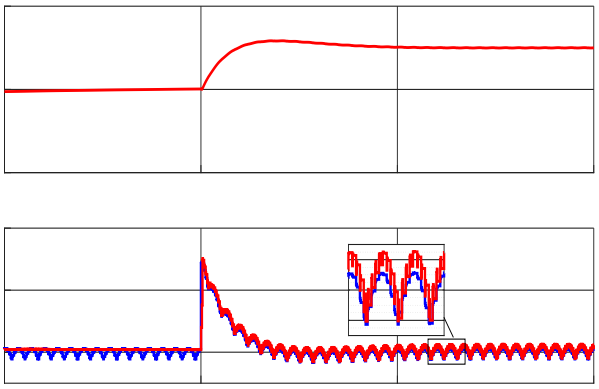

Figure 8. Converter 3 performance analysis – top: dc-link voltage control, bottom: *d*-axis current reference (blue) and feedback (red).

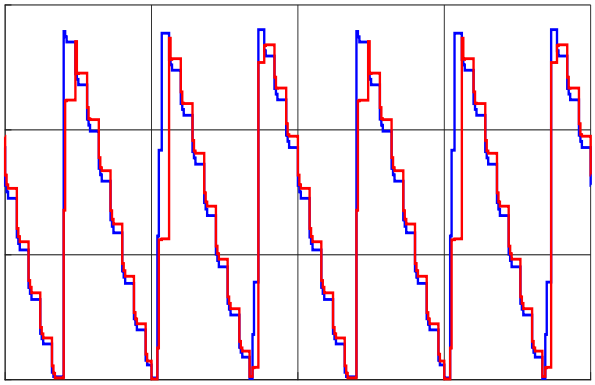

Figure 9. Converter 3 performance analysis – q-axis current control: reference current (blue) measured (red).

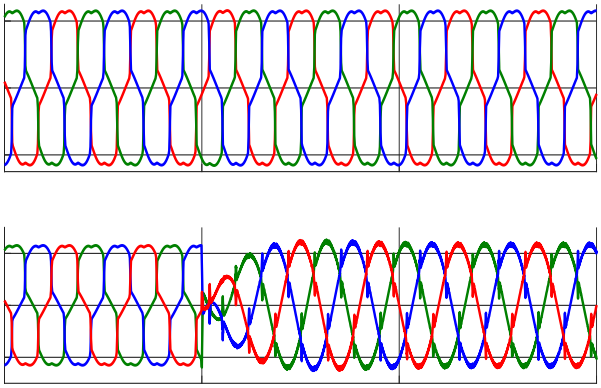

Figure 10. Current waveforms for feeder 3 – top: load 3 current, bottom: grid currents before and after compensation.

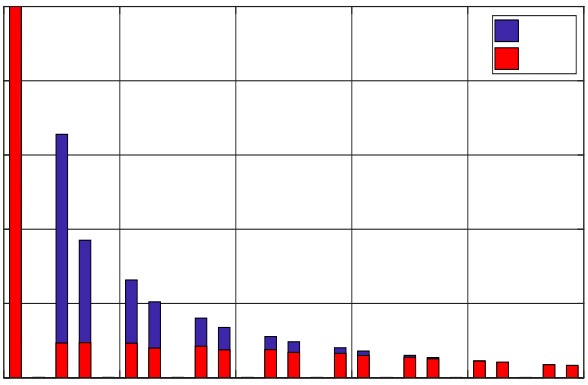

Figure 11. FFT analysis of grid currents at feeder 3 before and after compensation. THD before compensation: 17.9%, after: 6.18%.

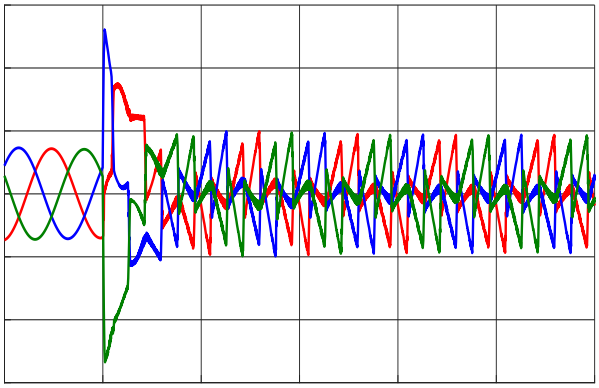

Figure 12. Converter 3 phase currents injected to compensate load current distortions – red: phase U, green: phase V, blue: phase W.

4.2. Experimental Results

The experiments are performed for the control of converter 3 only to verify its capability of compensating current distortion caused by non-linear loads. A diode bridge rectifier with a capacitive dc-link is used as load. A capacitive dc-link is chosen for its widespread use as input stage of modern variable speed drives. Fig. 13 shows the currents of phases U and V before and after compensation is enabled. An initial high amplitude of currents is due to the dc-link voltage being controlled to a higher value than that obtained through diode rectification of the bidirectional switches of converter 3. Fig. 14 shows the FFT of phase U currents before and after compensation. As can be seen in this figure, the current THD after compensation has been significantly improved.

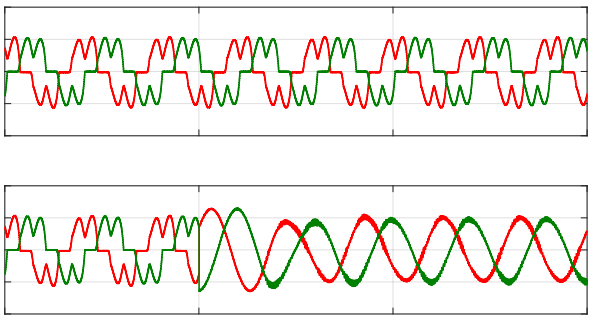

Figure 13. Experimentally observed phase U and phase V currents drawn from the grid before (top) and after (bottom) enabling current compensation at t = 0.05s for converter 3.

It can be noticed in Fig. 14 that the compensation does not improve the THD to make it under 5% (as recommended by power quality standards). Even though a fast deadbeat current control is implemented but due to the limited dc-link voltage, it is not possible to follow a highly distorted q-axis current reference (of Fig. 9). With a diode rectifier as load, it may be helpful to eliminate individual current harmonics by injecting compensation components in respective dq

reference frames rotating at harmonic frequencies. However, the physical constraint of limited dc-link voltage might not allow to compensate higher order harmonics.

Fig. 15 presents the phase voltages for phases U and V measured between the filter inductance L_f (of Fig. 2) and grid autotransformer. Before compensation, when currents of Fig. 13 (top plot) are drawn from the grid, the harmonically distorted currents flowing through the inductance of autotransformer cause voltage distortions at low frequency as seen in the FFT of Fig. 16. The voltages observed in Fig. 15 are typical of a weak microgrid that has low short-circuit capability that translates into higher input inductance (here demonstrated by the autotransformer). When the compensation is enabled, the low frequency harmonics are eliminated but higher frequency harmonics appear (red bars in Fig. 16). Even though converter 3 is supposed to compensate current harmonics only, the voltages are improved as a result of sinusoidal currents drawn from the grid.

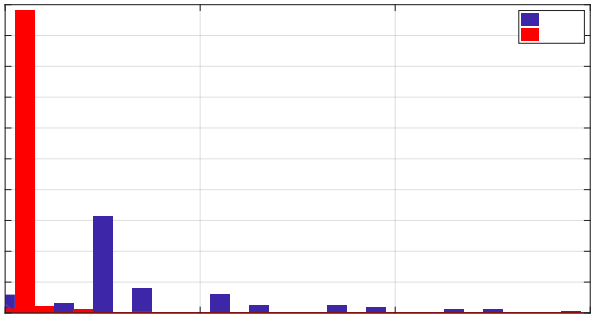

Figure 14. FFT comparison of phase U current before and after compensation of Fig. 13 is enabled. THD before compensation: 38.1%, after: 7.4%.

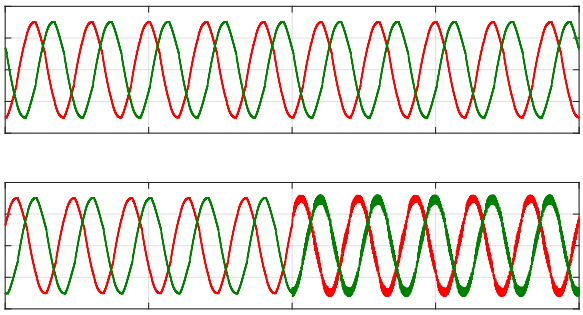

Figure 15. Experimentally measured phase U and phase V voltages between filter inductance and autotransformer output before (top) and after (bottom) enabling current compensation at t = 0.05s for converter 3.

5. Conclusions

In this paper, a power quality conditioner for distortion elimination in a weak ac microgrid is studied. The examined conditioner consists of three power electronic converters connected to a common dc-link. These compensate for the distortions in voltage and current caused by non-linear loads that may degrade the overall performance of the microgrids. Of all the three converters, the control of shunt power conditioner is given more attention as it needs to keep a constant dc-link voltage for proper functioning. A fast deadbeat controller is proposed that has the ability to inject high frequency current harmonics to render the current drawn from the grid close to a smooth sinusoid. Performance of the three converters is analysed by considering a practical microgrid system along with common distortion types. The THD of voltages and currents before and after compensation demonstrate the effectiveness of the studied power quality conditioner.

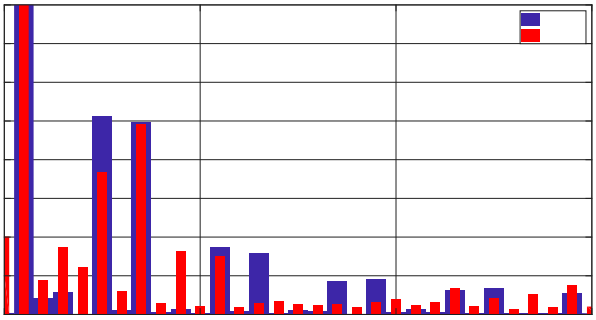

Figure 16. FFT comparison of phase U voltage before and after compensation of Fig. 13 is enabled.

References

[1] A. Kahrobaeian and Y. A.-R. I. Mohamed, "Interactive Distributed Generation Interface for Flexible Micro-Grid Operation in Smart Distribution Systems," *IEEE Trans. Sustain. Energy*, vol. 3, no. 2, pp. 295–305, Apr. 2012.

[2] T. Dragicevic, J. M. Guerrero, J. C. Vasquez, and D. Skrlec, "Supervisory Control of an Adaptive-Droop Regulated DC Microgrid With Battery Management Capability," *IEEE Trans. Power Electron.*, vol. 29, no. 2, pp. 695–706, Feb. 2014.

[3] F. Gao *et al.*, "Comparative Stability Analysis of Droop Control Approaches in Voltage-Source-Converter-Based DC Microgrids," *IEEE Trans. Power Electron.*, vol. 32, no. 3, pp. 2395–2415, Mar. 2017.

[4] D. Kumar and F. Zare, "Harmonic Analysis of Grid Connected Power Electronic Systems in Low Voltage Distribution Networks," *IEEE J. Emerg. Sel. Top. Power Electron.*, vol. 4, no. 1, pp. 70–79, Mar. 2016.

[5] J. M. Carrasco *et al.*, "Power-Electronic Systems for the Grid Integration of Renewable Energy Sources: A Survey," *IEEE Trans. Ind. Electron.*, vol. 53, no. 4, pp. 1002–1016, Jun. 2006.

[6] J. Eloy-García, J. M. Guerrero, and J. C. Vasquez, "Grid simulator for power quality assessment of micro-grids," *IET Power Electron.*, vol. 6, no. 4, pp. 700–709, Apr. 2013.

[7] C.-Y. Tang, Y.-F. Chen, Y.-M. Chen, and Y.-R. Chang, "DC-Link Voltage Control Strategy for Three-Phase Back-to-Back Active Power Conditioners," *IEEE Trans. Ind. Electron.*, vol. 62, no. 10, pp. 6306–6316, Oct. 2015.

[8] Y. Li, D. M. Vilathgamuwa, and P. C. Loh, "Microgrid Power Quality Enhancement Using a Three-Phase Four-Wire Grid-Interfacing Compensator," *IEEE Trans. Ind. Appl.*, vol. 41, no. 6, pp. 1707–1719, Nov. 2005.

[9] Z. Zeng, H. Li, R. Zhao, S. Tang, and H. Yang, "Multi-objective control of multi-functional grid-connected inverter for renewable energy integration and power quality service," *IET Power Electron.*, vol. 9, no. 4, pp. 761–770, Mar. 2016.

[10] P. Acuna, L. Moran, M. Rivera, J. Dixon, and J. Rodriguez,

"Improved Active Power Filter Performance for Renewable Power Generation Systems," *IEEE Trans. Power Electron.*, vol. 29, no. 2, pp. 687–694, Feb. 2014.

[11] T. Dragicevic, "Model Predictive Control of Power Converters for Robust and Fast Operation of AC Microgrids," *IEEE Trans. Power Electron.*, vol. 33, no. 7, pp. 6304–6317, Jul. 2018.

[12] Z. Xin, X. Wang, P. C. Loh, and F. Blaabjerg, "Grid-Current-Feedback Control for LCL-Filtered Grid Converters With Enhanced Stability," *IEEE Trans. Power Electron.*, vol. 32, no. 4, pp. 3216–3228, Apr. 2017.

[13] N. He *et al.*, "Weighted Average Current Control in a Three-Phase Grid Inverter With an LCL Filter," *IEEE Trans. Power Electron.*, vol. 28, no. 6, pp. 2785–2797, Jun. 2013.

[14] J. Dannehl, M. Liserre, and F. W. Fuchs, "Filter-Based Active Damping of Voltage Source Converters With LCL Filter," *IEEE Trans. Ind. Electron.*, vol. 58, no. 8, pp. 3623–3633, Aug. 2011.

[15] S. A. Khajehoddin, M. Karimi-Ghartemani, P. K. Jain, and A. Bakhshai, "A Control Design Approach for Three-Phase Grid-Connected Renewable Energy Resources," *IEEE Trans. Sustain. Energy*, vol. 2, no. 4, pp. 423–432, Oct. 2011.

[16] K. Jalili and S. Bernet, "Design of LCL Filters of Active-Front-End Two-Level Voltage-Source Converters," *IEEE Trans. Ind. Electron.*, vol. 56, no. 5, pp. 1674–1689, May 2009.

[17] A. Timbus, M. Liserre, R. Teodorescu, P. Rodriguez, and F. Blaabjerg, "Evaluation of Current Controllers for Distributed Power Generation Systems," *IEEE Trans. Power Electron.*, vol. 24, no. 3, pp. 654–664, Mar. 2009.

[18] P. Cortes, J. Rodriguez, C. Silva, and A. Flores, "Delay Compensation in Model Predictive Current Control of a Three-Phase Inverter," *IEEE Trans. Ind. Electron.*, vol. 59, no. 2, pp. 1323–1325, Feb. 2012.

[19] Y. Abdel-Rady Ibrahim Mohamed and E. F. El-Saadany, "An Improved Deadbeat Current Control Scheme With a Novel Adaptive Self-Tuning Load Model for a Three-Phase PWM Voltage-Source Inverter," *IEEE Trans. Ind. Electron.*, vol. 54, no. 2, pp. 747–759, Apr. 2007.

[20] Y. Liu and G. T. Heydt, "Power System Even Harmonics and Power Quality Indices," *Electr. Power Components Syst.*, vol. 33, no. 8, pp. 833–844, Aug. 2005.

[21] J. Barros, M. de Apráiz, and R. I. Diego, "Analysis of second order harmonic voltages in power systems," *Renew. Energy Power Qual.*, vol. 1, no. 05, pp. 163–167, Mar. 2007.